Modeling of CO_2 circulation in the Colli Albani area

MICOL TODESCO[1*]

*[1]Istituto Nazionale di Geofisica e Vulcanologia, Sezione di Bologna,Via Donato Creti, 12, 40127 Bologna, Italy *Corresponding author: todesco@bo.ingv.it*

GUIDO GIORDANO[2]

[2] Dipartimento di Scienze Geologiche, Università degli Studi di RomaTre, Largo S. Leonardo Murialdo, 1, 00146, Roma, Italy (e-mail: giordano@uniroma3.it)

Running title: Modeling of CO_2 circulation

Abstract

The Colli Albani is a quiescent volcano located nearby the city of Roma, characterised by the presence of an active geothermal system, periodic seismic swarms and intense diffuse degassing. Several accidents, some of which lethal, have occurred in recent years associated to episodes of more intense releases and outbursts of volcanic gases, dominantly CO_2 and H_2S. Gas emissions are presently the most hazardous phenomenon for the highly populated Colli Albani area, along with the potential occurrence of seismic activity. This chapter presents the numerical modeling of heat and fluid circulation applied to study the mechanisms which control the diffuse degassing at Colli Albani volcano. Multi-phase and multi-component simulations were carried out using the TOUGH2 geothermal simulator in a realistic geological context, which includes all available information on the stratigraphy and structure of the Colli Albani substrate, along with data on the total gas flux, the local geothermal gradient, the local hydrogeology, and the thermal characteristics of the rocks. The geothermal reservoir at Colli Albani is hosted by the 2-3000 m thick Mesozoic-Cenozoic carbonatic succession capped by Pliocene clays which act as aquiclude and are few hundreds to over 1000m thick, in turned covered by continental sedimentary and volcanic deposits, which host the shallow hydrogeological system. Numerical simulations evaluate the effects associated with the thickness of the carbonatic basement and its cap rock; the role of CO_2 supply rate at depth; and the influence of permeable channelways through the cap rocks. Numerical simulations show that thickness of the geothermal reservoir hosted by the carbonatic basement and of its impervious cover control the vigor of the convection, the extent and depth (and hence temperature) of the lateral recharge area, and the distribution of the carbon dioxide within the system. This result suggests that the temperature distribution and diffuse degassing at surface do not simply reflect the characteristics of

the heat and fluid source at depth, but also the specific structure and hydrological properties of the site where they are measured.

End of Abstract

The Colli Albani volcano is a Quaternary volcanic field located nearby the city of Roma (Fig. 1). No eruptions took place during historical times, but the volcano has been recently reclassified as quiescent based on documented Holocenic phreatic activity associated with the Albano maar lake (Funiciello *et al.* 2003; De Benedetti *et al.* 2008). In recent times, its state of activity has been characterized by periodic seismic swarms and ground deformation (Amato *et al*. 1994; Amato & Chiarabba 1995; Chiarabba *et al.* 1997). Diffuse degassing is also common in the area and, at some location, can induce significant health hazard (cf. Chiodini & Frondini 2001; Carapezza *et al*. 2003, 2010, this volume; Cioni *et al*. 2003; Carapezza & Tarchini 2007; Barberi *et al.* 2007; Voltaggio & Spadoni 2009). Gas emissions mostly consist of CO_2, which is abundant in groundwater, but H_2S, N_2, and CH_4 are all present in variable amounts. Rn activity is also very high in the zones where CO_2 emission occurs. The isotopic composition of carbon and the relatively high $^3He/^4He$ ratio (0.68-1.46) indicate a deep origin, associated with magma or mantle degassing and with metamorphic reactions. Measurements of diffuse CO_2 degassing have been carried out at different locations (Fig. 1; Chiodini & Frondini 2001; Beaubien *et al.* 2003; Carapezza *et al.* 2003). At Cava dei Selci a total amount of 95.7 ton/day has been measured over an area of 12000 m^2, corresponding to ca. $9x10^{-5}$ kg/m^2s. Other areas of relevant gas release are La Zolforata ($1x10^{-5}$ kg/m^2s) and Vigna Fiorita, where the removal of the impervious lahar cover led to CO_2 flux up to $6x10^{-4}$ kg/m^2s. Gambardella *et al.* (2004) performed a detailed analysis of the CO_2 flows in central Italy, and identified a deep carbon component for the Colli Albani volcanic district that was quantified in $2.54x10^6$ mol/km^2yr, corresponding to $9.7\ x10^{-10}$ kg/m^2 s.

Geochemical data indicate the presence of a pressurised, CO_2-rich gas reservoir, likely hosted in the aquifers beneath and within the volcanic cover. The accidental bursts of a shallow geothermal well, in 1986, and during the drilling of some water wells (Carapezza & Tarchini 2007; Barberi *et al.* 2007) corroborate the existence of such pressurised system. Sudden releases of CO_2, and rapid heating of water springs have also been reported in relation to seismic events (Funiciello *et al.* 2003; Tuccimei *et al.* 2006).

Emissions are present also near and within the Albano lake, where volcanic gases percolate through the lake bottom and dissolve into the lake waters at depth (Anzidei *et al.* 2008). The CO_2 storage in

the lake's water is associated with a potential (although not impending) hazard, as testified by the presence of lahar deposits related to lake overflows (cf. Tavolato Formation; Giordano *et al.* 2010, this volume; Funiciello *et al.* 2003; De Benedetti *et al.* 2008).

In this work, numerical modeling of heat and fluid circulation was applied to study the mechanisms controlling diffuse gas emissions at the Colli Albani volcano. Simulations were carried out to evaluate conditions favoring the ascent and exsolution of carbon dioxide from the carbonatic basement up to the shallow volcanic series hosting the water table. Numerical simulations evaluate the effects associated with the thickness of the carbonatic basement and its cap rock; the role of CO_2 supply rate at depth; and the influence of permeable channelways through the cap rocks (Table 1). The resulting reservoir conditions and degassing rate at the surface are compared for the different cases.

Preliminary results show that overall fluid circulation and surface CO_2 emissions are highly affected by the thickness and physical properties of the carbonatic basement that acts as the main geothermal reservoir.

The geological-hydrogeological framework

The ascent and propagation of deep-seated gases is controlled by the rate at which they are generated at depth, but also depend on the hydrogeological properties of the rocks through which they flow. The reconstruction of the Colli Albani geology is described in Mattei *et al*. 2010 (this volume) and Giordano *et al.* 2010 (this volume; cf. Giordano *et al.* 2006; Bianchi *et al*. 2008), whereas the hydrogeology in Mazza & Capelli 2010 (this volume; cf. Boni *et al.* 1995; Capelli *et al*. 2006). The permeable volcanic edifice overlies a regional aquiclude, several hundreds meters thick, made of alternating marine clay and sand belonging to the Pliocene-Quaternary post-orogenic succession. This formation represents the main cap rock. A highly permeable Meso-Cenozoic carbonatic succession forms the basement and the main geothermal reservoir for the area (Chiodini & Frondini, 2001; Gambardella *et al.* 2004; Carapezza & Tarchini, 2007) (Figure 2). This basement is affected by syn-orogenic thrust tectonics and post-orogenic extensional tectonics forming structural highs and lows (Fig. 2) that are clearly identified from gravity data (Fig. 1; Mattei *et al.* 2010, this volume; Di Filippo & Toro, 1995). Gas emissions are usually associated with structural highs that act as traps, and with local tectonic discontinuities that represent preferential pathways for fluid ascent. The geothermal system is sustained by the Colli Albani magma chamber, which is

located largely below and partly within the carbonatic series (cf. Conticelli *et al*. 2010, this volume).

Numerical model and computational domain

The fluid circulation at Colli Albani was simulated with the TOUGH2 geothermal simulator (Pruess *et al.* 1999). This multi-phase and multi-component model describes the coupled flow of heat and fluids through heterogeneous porous media. In the present application, the considered fluid components are water and carbon dioxide. The model accounts for the dissolution of carbon dioxide in liquid water according to Henry's law, and describes water phase change as a function of system conditions.

All the geological, geophysical, geochemical, and hydrogeological information available for the Colli Albani region have been considered in order to provide a reliable description of the underground rock sequence, with the most relevant porous domains. Physical and hydraulic properties assigned to each rock units are reported in Table 2. Two schematic stratigraphic sequences were defined to represent typical conditions of structural high and low (Fig. 3).

The computational domain and boundary conditions are shown in Fig. 4. The domain is initially cold and water saturated. Heat (0.1 W/m^2) and hot (ca. 350°C) carbon dioxide (10^{-9} kg/m^2s) are injected along the base of the domain until the steady state is reached, for each of the two considered rock sequences (Simulations 1 & 2). Heating and fluid flow prompt a vigorous convection within the permeable carbonatic basement, for both structural settings (Fig. 5). At steady state, a wide, clockwise convective cell occupies the entire basement ,while negligible fluid motion occurs at shallower depths (Fig. 5b,d). The carbon dioxide released at the bottom dissolves in the water, rises along the symmetry axis and accumulates at the base of the low-permeability clay layer. Hot water propagates outward, along the base of the clay, and finally leaves the domain through its outer boundary, 10 km from the symmetry axis. Recharge of cold, liquid water occurs through the same vertical boundary at greater depths. With time, carbon dioxide penetrates within the clay layer and slowly propagates forming a wide plume. Eventually, in both simulations some minor fractions of CO_2 (0.06) exsolve to form a water-dominated two-phase region, delimited by

the thick, black line in Fig. 5(b,d). Diffuse degassing takes place where the gas phase develops, as shown in Figs 5a & 5c. Although the evolution in the two considered cases is qualitatively similar, the different geometries associated with the structural high and structural low cause some significant differences. The thinner basement in Simulation 2 prompts a more vigorous convection. Carbon dioxide is more effectively diluted and reaches a lower concentration within the plume. The thicker Clay layer hinders the ascent of carbon dioxide toward the surface, and the resulting degassing rate does not exceed 0.2×10^{-9} kg/m^2 s. On the contrary, carbon dioxide concentrates in the case of structural high, and achieves higher partial pressures (up to 5 MPa at steady state) (Fig. 5b). The higher CO_2 enrichment in turn leads to the development of a wider two-phase zone and stronger degassing rate at the surface (up to 0.8×10^{-9} kg/m^2 s). The structural setting also affects the temperature distribution within the system at steady state (Fig. 6). In both the considered cases, the shallow layers above the impermeable clay are heated mostly by conduction, and remains colder, whereas the permeable basement is effectively heated by convection. In the case of structural high, convection carries heat over a wider portion of the domain; at the same time, the outer boundary is permeable over a larger fraction of its length, allowing an effective recharge of cold water. As a result, temperatures in excess of 150°C are found at depths shallower than 1000 m, but never exceeded (Fig. 5a). In the case of structural low, higher maximum temperatures are achieved (200°C), but are confined to greater depths, within the carbonatic basement. A more uniform and effective heating is ensured by the thicker cap rock, the more vigorous convection, and the smaller recharge area along the outer boundary (Fig. 5b).

Steady state conditions can be also examined in terms of vertical profiles of selected variables. Figure 7 shows the distribution of CO_2 partial pressure, temperature, and gas fraction with depth, along the symmetry axis. The comparison of the profiles associated with the two structural settings clearly show how the same boundary conditions result into different distribution of the variables at steady state. The structural high (dashed line) is characterized by higher values of CO_2 partial pressure and of gas saturation at all depths. The temperature profiles clearly identify the deep, isothermal region dominated by convection, and the shallow conductive layers, characterized by a strong thermal gradient, for both cases considered. The structural high (dashed line) is hotter from the surface to the base of the clay layer, and with a lower temperature within the basement. A thicker two-phase region is present in the case of structural high, but the maximum gas saturation is similar in the two cases, and always very low (0.06).

System perturbation: (1) the fluid source at depth

Starting from the steady system conditions described above, some perturbations were imposed, to evaluate their effects on phase distribution and surface degassing.

The first perturbation is related to the rate of CO_2 generation at depth (Simulations 3 & 4). A stronger CO_2 injection rate (10^{-7} kg/m^{2}s) is imposed near the symmetry axis to represent a localized inlet (100 m wide) of magmatic volatiles (Fig. 8a). The gas flow rate along the rest of the bottom boundary remains unchanged (10^{-9} kg/m^{2}s). Heat flow is fixed at 0.1 W/m^2 along the entire boundary, as in Simulations 1 & 2. The same boundary conditions shown in Fig. 4 are applied once again to both the considered structural domains.

Figure 9 illustrates the temporal evolution of the carbon dioxide partial pressure in the case of structural high (a-c) and structural low (d-f). In both cases, the system evolution is very slow, despite the high permeability assigned to the carbonatic basement. The larger CO_2 injection at the inlet (white arrows) progressively increases the amount of carbon dioxide that propagates along the symmetry axis. After 10,000 years, and for the structural high (Fig. 9a), most of the gas accumulates within the permeable basement whereas minor amounts propagate through the low-permeability clay layer. At this time, some fraction (0.036) of gas (thick, black line) develops underneath the clay (at -800 m depth) near the symmetry axis. As the slow propagation through the shallow layers proceeds, the amount of gas increases progressively. At steady state (ca. 1 Ma, Fig. 9c), a funnel-shaped two-phase zone has developed from the surface down to a maximum depth of about 900 m (black line), with a maximum gas fraction of about 0.09. The CO_2 partial pressure within the shallow clay layer has reached ca. 8 MPa.

The evolution in case of structural low is qualitatively similar (Fig. 9 d-f). The carbon dioxide rises along the symmetry axis and spreads out along the base of the clay. The higher pore pressure at this depth prevents the development of a gas phase at the base of the clay. A slow propagation takes place through the clay layer where the CO_2 partial pressure is as high as 7 MPa at steady state. Gas exsolution at shallower depths contributes to increase the size of the two-phase zone that, in this case, reaches but does not penetrate the top of the clay layer, at 400 m depth.

The stronger activity of the CO_2 source at depth increases the overall amount of gas within the system. It is interesting to observe how the properties of the shallow layers affect the distribution of the gas phase, which tend to concentrate within the less permeable strata (Fig. 10). This behavior is associated with the mobility of the two phases, which in turn depends on their saturation. As the gas

phase occupies only a minor fraction of the pore volume (its saturation is always below 0.1), its mobility is reduced by the pervasive presence of liquid water. For this reason, once the gas reaches a low-permeability layer, it tends to become immobile and it accumulates, as new gas ascend from below.

The stronger CO_2 source affects the variables distribution and degassing rate at steady state (Fig. 11). The CO_2 partial pressure along the symmetry axis (Fig. 11a) increases at all depths, for both structural settings, but the temperature profiles (Fig. 11b) are not affected by the stronger activity of the source. The volumetric gas fraction undergoes major changes, especially in the case of structural high, where gas saturation reaches larger values over a wider range of depths (Fig. 11c). Maximum values of gas saturation highlight the presence of less permeable layers in both simulations. The increment in gas fraction is also associated with a higher degassing rate at the surface, up to 1.1×10^{-9} kg/m^{2}s in the case of structural high (Fig. 11d). The effect of the source at depth is mostly confined to the axial region, above the location of the "magmatic" source.

System perturbation: (2) opening through the impervious layers

Further simulations were run to evaluate the effects of a discontinuity of the impervious layers. In the first case (Simulations 5 & 6), the shallow Pisolitic Tuff layer is interrupted near the symmetry axis (Fig. 8b), whereas in the second case (Simulations 7 & 8) the gap affects the thicker and deeper Clay layer (Fig. 8c). These gaps could be due to a non-uniform sedimentation, or to a fault or fracture zone.

Simulation 5 refers to the case in which the shallow Pisolitic layer is interrupted and the rock sequence corresponds to a structural high. Initial conditions are taken from the steady state achieved in Simulation 1. The presence of the gap influences the circulation within the permeable, upper layer (Fig. 12a): within 10 years, the faster fluid ascent through the gap drives a vigorous convection. This favors the circulation of cold, liquid water (available all along the upper boundary that is water saturated and held at constant, atmospheric conditions). As a result, the two-phase zone is gradually disrupted within the upper layer. This evolution is reflected by the rate of diffuse degassing through the surface (Fig. 12b): initially, diffuse degassing is enhanced, as larger amounts of carbon dioxide propagate through the gap and reach the surface of the domain. With time, however, the liquid water permeates the shallow layer, hindering the gas ascent. At steady state (201

kyr), surface degassing is absent near the symmetry axis. Steady state conditions do not change significantly if the simulation is run from cold and CO_2-free initial conditions (i.e. if the gap existed since the deposition of the impermeable layer).

Although the fluid flow pattern changes significantly, with respect to the initial conditions, these changes are confined at a very shallow depth, and do not affect the overall temperature distribution within the system. The case of structural low (Simulation 6, not shown) is characterized by a similar evolution, with liquid water permeating the upper layer, and limiting surface degassing.

The second set of simulations is performed with a gap affecting the impermeable Clay layer at depth. Figure 13 illustrates the temporal evolution of the volumetric gas fraction, for the case of structural high (Simulation 7). The thin vertical channel allows the ascent of deep seated fluids that add to the shallow two-phase region. Carbon dioxide accumulates at the base of the Pisolitic Tuff layer (continuous, in this case) and, with time, affects the circulation within the upper layer as well. As a result, the two-phase region is once again partially disrupted at steady state (994 kyr, in this case). The ascent of deep-seated fluids modifies the temperature distribution within the system. Heating affects the entire permeable channel and temperatures in excess of 100°C are found at depths of 400 m (Figure 14a). Surface degassing increases significantly during the entire simulation. In particular, flow rates at the symmetry axis reaches values as high as $6x10^{-8}$ kg/m^{2}s.

In case of structural low (Simulation 8), the evolution is similar, but lower amounts of gas reach the shallow two-phase region (Figure 15a). This reflects on the circulation within the upper layer where the two-phase region survives to steady state (553 kyr). Fluid ascent is accompanied by heating, although slightly lower values are reached (Figure 15 b). Diffuse degassing increases throughout the simulation to a maximum value of $8x10^{-9}$ kg/m^{2}s. Figure 16 illustrates the overall changes associated with the permeable channel: the two-phase region increases significantly for both settings, and the new pattern of circulation affects the overall distribution of carbon dioxide. Heating at shallow depths is also evident from the vertical profile, and indicates the contribution of fluid flowing through the permeable channel.

Discussion and Conclusions

The Colli Albani volcano, although quiescent, has been the site of several accidents associated with CO_2 and H_2S degassing, some of which were lethal (Carapezza *et al.* 2003, 2010; Carapezza & Tarchini 2007). The deep origin of the gases calls for a comprehensive conceptual model of the geothermal field that underlies the volcano. However, early geothermal exploration at Colli Albani

was dismissed after low temperatures (41°C at 610 m depth) were detected in a deep-well drilled in Falcognana, in 1986 (ENEL, 1990; see Danese & Mattei 2010, this volume). Low temperatures are consistent with the relatively low heat flow measured in the region, as compared to the higher values characterising the nearby high-enthalpy geothermal areas, in Northern Latium (Mongelli *et al*. 1991). Other pieces of information derive from the observation of diffuse degassing and contribute to our current knowledge of the geothermal system: it is widely acknowledged that diffuse degassing mostly occurs at structural highs (Fig. 1); CO_2 is known to exist as a free gas phase, at various depths below impervious layers (Carapezza & Tarchini 2007; Barberi *et al.* 2007); sudden releases of gas or hot fluids have been observed in association with local or distal earthquakes, although the relation between the two phenomena is not univocal.

The low temperatures and the common occurrence of diffuse degassing in the area have been traditionally explained assuming an efficient recharge of the aquifer within the carbonatic basement. Fresh water from the Apennines can quickly propagate through fast, karstic circuits and dilute the deep geothermal component (e.g. Duchi *et al*. 1991; Giggenbach *et al*. 1988; Chiodini & Frondini 2001). This interpretation is still mostly based on qualitative considerations. The first work aimed at a quantitative assessment of diffuse degassing at the scale of the volcano is still that by Chiodini & Frondini (2001), who interpolated data of CO_2 concentration in groundwater for the western, southern, and central portion of the volcano. Based on those data, Gambardella *et al.* (2004) attempted a calculation of the total gas release from the volcano. Other works focused on limited areas of more intense degassing where accidents have occurred in the recent past, such as Cava dei Selci, La Zolforata and the Albano Lake (Carapezza *et al.* 2003, 2010; Annunziatellis *et al.* 2003; Beaubien *et al.* 2003; Carapezza & Tarchini 2007; Barberi *et al.* 2007).

Our work provides a first-order, quantitative framework to understand the Colli Albani geothermal/ hydrogeological system and its relationship to diffuse degassing. A first result is related to the role of the structural setting of the area. Numerical simulations show that thickness of the carbonatic basement and of its impervious cover control the vigor of the convection, the extent and depth (and hence temperature) of the lateral recharge area, and the distribution of the carbon dioxide within the system. Simulations performed considering different structural settings end up with different geothermal gradients and degassing rates, even though boundary conditions are the same. In particular, the structural high is characterised by lower temperature in the basement (ca. 150°C), and by a steeper thermal gradient at shallower depths (Figs 6 and 7). Carbon dioxide is efficiently

conveyed toward the surface, and the resulting degassing rate is 4 times higher than in case of structural low (Fig. 5).

This result is relevant, as it suggests that data on the temperature distribution or diffuse degassing do not simply reflect the characteristics of the heat and fluid source at depth, but also the specific structure and hydrological properties of the site where they are measured. Our simulations are based on two ideal stratigraphic sequences that do not correspond to any specific location in the area. For this reason, we did not expect to match any specific data set. Nevertheless, the simulations confirm that structural highs are associated with stronger degassing (comparable with the estimates by Gambardella *et al.* (2004), and imply that low temperature in the main reservoir do not necessarily relate to a lack of a heat source at depth.

Surface degassing certainly depends on the strength of the gas source at depth. A stronger input at the base reflects into a larger degassing rate at the surface (Fig. 11). Also in this case, the rate at which carbon dioxide is released at the surface changes with the structural setting and is larger in the case of structural high. The stronger input also causes an enlargement of the two-phase region, and an increase of the gas fraction, especially within the less permeable layers. For the system properties and conditions considered here, however, the maximum gas fraction achieved is always very low, and the gas phase never saturates the pore space. Slight pressurisation (up to $+0.6 \times 10^5$ Pa) occurs at shallow depths (<500 m) where the gas fraction increases, for both structural settings.

Another interesting consideration arises from the simulated times. Changes imposed at the base of the domain require very long times to reach the surface (of the order of thousands of years). These times are not consistent with the occurrence of sudden changes (either in temperature and/or in flow rate) that were observed at various emission points in the area. This discrepancy suggests that either these fast changes occur where local rock properties allow a faster fluid migration, or they are are driven by a much shallower source, such as a change in the hydraulic properties of the cap rocks.

In our simulations, the continuity of impervious layers is a fundamental key that controls the shallow fluid circulation. A gap in the shallow pisolitic layer introduces major changes in the gas fraction and phase distribution below the surface (Fig. 12). Degassing increases more than one order of magnitude even if the rate of CO_2 generation at depth has not changed. In our simulation, the gap in the impervious layer is filled by the underlying sand. This situation is meant to describe a damaged, or fracture zone, or an impervious layer that was originally discontinuous. Drilling of a water well would actually remove the porous rock and suddenly place the gas at the well head under

atmospheric pressure. This process, not simulated here, is expected to have an even larger impact on the dynamics of gas expansion and ascent, as shown by recent accidents in the area.

Our results also show, that with time, the circulation triggered by the uprising fluids culminate with flooding of the shallowest rock layer. As a result, degassing ceases where rocks become water saturated (Fig. 12). This particular phenomenon is due to the boundary conditions imposed along the top, which allow a continuous feeding of cold water at the surface. Even if not realistic, this behaviour well illustrates the sensitivity of surface degassing to the presence of liquid water. It is reasonable to expect that drying of a shallow aquifer could result into a remarkable increase in gas emissions, which would be totally unrelated to the state of the volcano.

Finally, our results show that major effects are observed if a gap exists through the main cap rock of the reservoir at depth. Hot, CO_2-rich fluids can propagate through the clay thanks to a permeable channel way, and freely expand within the shallow layers. As a result, not only the emission rate at the surface increases significantly (Figs 14, 15 & 16), but also the temperature distribution is affected to shallow depths.

This result is consistent with the findings of high CO_2 partial pressure reported within the NE-SE trending Ardea graben. This area contradicts the usual trends by which major degassing occur at structural highs. The Ardea graben, however, is an active tectonic area, and degassing could be associated to fracturing which may dissect the Pliocene clay aquiclude (Faccenna *et al.* 1994).

Although preliminary, our results are consistent with the data and suggest that, upon appropriate calibration, the model could provide important insights on the mechanism controlling diffuse degassing. Future improvements should involve the simulation of complex 3D domains, describing both structural highs and lows within the same simulation. Our results stress the need for a detailed definition of the rock properties and of the subsurface rock sequences, in order to define location, size, and geometry of aquicludes and permeable regions.

The integration of geophysical, volcanological, and monitoring data into a consistent physical model represents a very promising approach to both scientific and civil defense issues.

References

AMATO, A. & CHIARABBA, C. 1995. Earthquake occurrence and crustal structure. In: Trigila, R. (ed) *The* Volcano *of the Alban Hills*. Tipografia SGS, Roma, 193-211.

AMATO, A., CHIARABBA, C., COCCO, M., DI BONA, M. & SELVAGGI, G. 1994. The 1989-1990 seismic swarm in the Alban Hills volcanic area, central Italy. *Journal of Volcanology and Geothermal Research,* **61**, 225-237.

BARBERI, F., CARAPEZZA, M. L., RANALDI, M. & TARCHINI, L. 2007. Gas blowout from shallow boreholes at Fiumicino (Rome): Induced hazard and evidence of deep CO2 degassing on the Tyrrhenian margin of Central Italy. *Journal of Volcanological and Geothermal Research*, **165**, 17-31.

BEAUBIEN, S. E., CIOTOLI, G. & LOMBARDI, S. 2003. Carbon dioxide and radon gas hazard in the Alban Hills area (central Italy). *Journal of Volcanological and Geothermal Research,* **123**, 63-80.

BIANCHI, I., PIANA AGOSTINETTI, N., DE GORI, P. & CHIARABBA, C. 2008. Deep structure of the Colli Albani volcanic district (central Italy) from receiver functions analysis. *Journal of Geophysical Research*, **113**, B09313, doi:10.1029/2007JB005548.

BONI, C., BONO, P., LOMBARDI, S., MASTRORILLO, L. & PERCOPO, C. 1995. Hydrogeology, fluid geochemistry and thermalism. In: Trigila, R. (ed) *The* Volcano *of the Alban Hills*. Tipografia SGS, Roma, 221–242.

CAPELLI, G., MAZZA, R. & GAZZETTI, C. 2006. *Strumenti e strategie per la tutela e l'uso compatibile della risorsa idrica nel Lazio: gli acquiferi vulcanici*. Pitagora Editrice, Bologna, 191 p.

CARAPEZZA, M. L., BADALAMENTI, B., CAVARRA, L. & SCALZO, A. 2003. Gas hazard assessment in a densely inhabited area of Colli Albani Volcano (Cava dei Selci, Roma). *Journal of Volcanological and Geothermal Research*, **123**, 81–94.

CARAPEZZA, M.L, BARBERI, F., TARCHINI, L., RANALDI, M. & RICCI, T. 2010. Volcanic hazard of Colli Albani. *In*: FUNICIELLO, R. & GIORDANO, G. (eds) *The Colli Albani Volcano*. Special Publication of IAVCEI, **3**. The Geological Society, London, 000-000.

CARAPEZZA, M. L., & TARCHINI. L. 2007. Magmatic degassing of the Alban Hills volcano (Rome, Italy): geochemical evidence from accidental gas emission from shallow pressurized aquifers. *Journal of Volcanological and Geothermal Research*, **165**, 5–16.

CHIARABBA, C., AMATO, A. & DELANEY, P. T. 1997. Crustal structure, evolution, and volcanic unrest of the Alban Hills, central Italy. *Bulletin of Volcanology*, **59**, 161-170.

CHIODINI, G., & FRONDINI, F. 2001. Carbon dioxide degassing from the Albani Hills volcanic region, Central Italy. *Chemical Geology*, **177**, 67-83.

CONTICELLI, S., BOARI, E., AVANZINELLI, R., DE BENEDETTI, A. A. , GIORDANO, G., MATTEI, M., MELLUSO, L. & MORRA, V. 2010. Geochemistry, isotopic composition and petrogenetic modelling of the Colli Albani volcanic rocks. *In*: FUNICIELLO, R. & GIORDANO, G. (eds) *The Colli Albani Volcano*. Special Publication of IAVCEI, **3**. The Geological Society, London, 000-000.

DANESE, E. & MATTEI, M. 2010. The sedimentary substrate of the Colli Albani volcano. *In*: FUNICIELLO, R. & GIORDANO, G. (eds) *The Colli Albani Volcano*. Special Publication of IAVCEI, **3**. The Geological Society, London, 000-000.

DE BENEDETTI, A. A., FUNICIELLO, R., GIORDANO, G., DIANO, G. CAPRILLI, E. & PATERNE, M. 2008. Volcanology, history and myths of the Lake Albano maar (Colli Albani volcano, Italy). In CASHMAN K. & GIORDANO G. (eds) *Volcanoes and Human History*. Journal of Volcanological and Geothermal Research, special issue, **176**, 387-406.

DI FILIPPO, M. & TORO, B. 1995. Gravity features. In: Trigila R. (ed): *The Volcano of the Alban Hills*, Tipografia SGS, Roma, 213-219.

DUCHI, V., PAOLIERI, M. & PIZZETTI, A. 1991. Geochemical study on natural gas and water discharges in the Southern Latium (Italy): circulation, evolution of fluids and geothermal potential in the region. *Journal of Volcanological and Geothermal Research*, **47**, 221-235.

ENEL, 1990. Esplorazione geotermica nel P.R. Colli Albani. Internal Report, Pisa, p. 54.

FUNICIELLO, R., GIORDANO, G. & DE RITA, D. 2003. The Albano Maar Lake (Colli Albani volcano, Italy): recent volcanic activity and evidence of pre-Roman Age catastrophic lahar events. *Journal of Volcanology and Geothermal Research*, **123**, 43-61.

GIGGENBACH, W.F., MINISSALE, A.A. & SCANDIFFIO, G. 1988. Isotopic and chemical assessment of geothermal potential of the Colli Albani area, Latium, Italy. *Applied Geochemistry*, **3**, 475–486.

GIORDANO, G. & THE CARG TEAM 2010. Stratigraphy and volcano-tectonic structures of the Colli Albani volcanic field. *In*: FUNICIELLO, R. & GIORDANO, G. (eds) *The Colli Albani Volcano*. Special Publication of IAVCEI, **3**. The Geological Society, London, 000-000.

GIORDANO, G., DE BENEDETTI, A.A., DIANA, A., DIANO, G., GAUDIOSO, F., MARASCO, F., MICELI, M., MOLLO, S., CAS, R. A. F. & FUNICIELLO, R. 2006. The Colli Albani mafic caldera (Roma, Italy): stratigraphy, structure and petrology, *Journal of Volcanology and Geothermal Research,* Spec. Iss. "Explosive mafic volcanism", **155**, 49-80.

MATTEI, M., CONTICELLI, S. & GIORDANO, G. 2010. The Tyrrhenian margin geological setting: from the Apennine orogeny to the K-rich volcanism. *In*: FUNICIELLO, R. & GIORDANO, G. (eds) *The Colli Albani Volcano*. Special Publication of IAVCEI, **3**. The Geological Society, London, 000-000.

MAZZA, R. & CAPELLI, G. 2010. Hydrogeology of the Colli Albani volcano. *In*: FUNICIELLO, R. & GIORDANO, G. (eds) *The Colli Albani Volcano*. Special Publication of IAVCEI, **3**. The Geological Society, London, 000-000.

MONGELLI, F., ZITO, G., CATALDI, R. et al. 1991. *Geothermal regime of Italy and surrounding seas,* in *Terrestrial Heat Flow and the Lithosphere Structure* (eds. V. Cermák and L. Rybach). Springer-Verlag, Berlin/Heidelberg, pp. 381–394.

PRUESS, K., OLDENBURG, C.M. & MORIDIS, G. 1999. TOUGH2 User's Guide, Version 2.0, Report LBNL-43134, Lawrence Berkeley National Laboratory, Berkeley, California

TUCCIMEI, P., GIORDANO, G. & TEDESCHI, M. 2006. CO_2 release variations during the last 2000 years at the Colli Albani volcano (Roma, Italy) from speleothems studies. *Earth and Planetary Science Letters*, **243** (3-4), 449-462.

VOLTAGGIO, M. & SPADONI, M. 2009 Mapping of H_2S fluxes from the ground using copper passive samplers: An application study at Zolforata di Pomezia degassing area. *Journal of Volcanological and Geothermal Research*, **179**, 56-68.

Table 1

Simulation	Feeding rate	Structural settings	Impervious layers
1	10^{-9} kg/m^{2}s	High	Continuous
2	10^{-9} kg/m^{2}s	Low	Continuous
3	10^{-7} kg/m^{2}s	High	Continuous
4	10^{-7} kg/m^{2}s	Low	Continuous
5	10^{-9} kg/m^{2}s	High	Gap through Pisolitic Tuffs
6	10^{-9} kg/m^{2}s	Low	Gap through Pisolitic Tuffs
7	10^{-9} kg/m^{2}s	High	Gap through clay
8	10^{-9} kg/m^{2}s	Low	Gap through clay

Table 2

Rock type	Density (kg/m^3)	Porosity	Permeability (m^2)	Heat conductivity (W/m°K)	Specific heat (J/kg°K)
Volcanics	2000	0.45	10^{-12}	0.8	900
Pisolitic Tuffs	1500	0.35	10^{-15}	0.8	900
Sand	2300	0.25	10^{-14}	2.0	1000
Clay	1750	0.35	10^{-17}	1.5	1000
Carbonate	2800	0.1	10^{-12} - 10^{-14}	1.1	900

Figure Captions

Fig. 1. DEM of the Colli Albani volcano and the regional Bouguer gravimetry (from Di Filippo & Toro 1995). The stars highlight sites where high diffuse degassing has been measured: 1: Acquacetosa; 2: Acqua S. Paolo (Laurentina); 3; Cava dei Selci; 4; S. Maria delle Mole; 5: Fosso

dell'Acqua Rossa; 6; Albano Lake; 7; La Zolforata; 8: Ardea; 9: Tor Caldara (modified from Giordano *et al.* 2006).

Fig. 2. Geologic section through the Colli Albani volcano. with structural high and lows (modified from Carapezza & Tarchini 2007).

Fig. 3. Schematic sequence of rock types implemented to represent structural high (a) and low (b) in the simulations. Different lithologies, characteristic of the area, are listed in the legend. Numbers refer to depth (m) below sea level.

Fig. 4. Two-dimensional, axisymmetric computational domain and boundary conditions. The computational grid is composed by 1534 elements with radial dimension ranging from 50 to 1500 m, and vertical dimension from 10 to 200 m. Fixed values of the primary variables are assigned along the open boundaries, and correspond to atmospheric pressure and temperature along the top, and to the initial pressure and temperature distribution, along the vertical boundary. Prescribed heat and CO_2 flows are imposed along the bottom.

Fig. 5. Steady state conditions for simulations 1 & 2. Gas flow rate (kg/m^2s) along the surface (a, c) and distribution of the CO_2 partial pressure (MPa) (b, d), for the cases of structural high (a, b) and low (c, d). Vectors highlight the pattern of liquid flow. Contour lines every 0.5 MPa, from 1 to 5 MPa. These conditions are taken as initial conditions for the following simulations.

Fig. 6. Steady state conditions for simulations 1 & 2 simulations 1 & 2. Temperature (°C) distribution for structural high (a) and low (b). Contour lines every 10°C, from 30 to 180°C. Steady state conditions are taken as initial conditions for the following simulations. Different patterns indicate lithologies, as shown in Fig. 3.

Fig. 7. Simulations 1 & 2. Distribution of (a) CO_2 partial pressure (MPa), (b) temperature (°C), and (c) volumetric gas fraction versus depth, along the symmetry axis. Dashed line: structural high; solid line: structural low.

Fig. 8. Boundary conditions for Simulations 3 to 8. (a) Size, flow rate, and location of carbon dioxide sources along the bottom (Simulations 3 & 4); (b) size and position of the gap through the impermeable Pisolitc Tuff layer (Simulations 5 & 6); (c) size and position of the gap through the impermeable clay layer (Simulations 7 &8).

Fig. 9. Simulations 3 & 4. Distribution of CO_2 partial pressure at different times for structural high (a,b,c) and low (d,e,f). Contour lines every 1 MPa, from 1 to 6 MPa. The thick black line indicates the extent of the two-phase zone. White arrows indicate the position of the inlet of magmatic fluids. Different patterns indicate lithologies, as shown in Fig. 3.

Fig. 10. Simulations 3 & 4. Distribution of volumetric gas fraction at steady state in the case of structural high (a) and low (b). Contour lines every 0.01, from 0.02 to 0.08. Different patterns indicate lithologies, as shown in Fig. 3.

Fig. 11. Simulations 3 & 4. Distribution of (a) CO_2 partial pressure (MPa), (b) temperature (°C), and (c) volumetric gas fraction versus depth, along the symmetry axis, at the beginning of the simulations and at steady state refer to steady state. (d) Gas flow rate along the surface at the beginning of the simulation and at steady state, for structural high and low.

Fig. 12 Simulation 5. (a) Volumetric gas fraction and flow pattern of liquid water, at different times. Contour lines every 0.005, from 0.02 to 0.065. Maximum flow rate of liquid water is 7.75×10^{-5} kg/m^2 s. Different patterns indicate lithologies, as shown in Fig. 3, and highlight the gap through the shallow Pisolitic Tuff layer. (b) Gas flow rate along the surface at different times.

Fig. 13. Simulation 7. Volumetric gas fraction and flow pattern of liquid water at shallow depths and at different times. Contour lines every 0.005, from 0.02 to 0.065. Maximum flow rate is 7.75×10^{-5} kg/m^2 s. Different patterns indicate lithologies, as shown in Fig. 3, and highlight the gap through the Clay layer at depth.

Fig. 14. Simulation 7. (a) Temperature (°C) distribution at steady state. Contour lines every 10°C, from 30 to 140°C. The thick, black line indicates the extent of the two-phase zone. (b) Gas flow rate along the surface at different times.

Fig. 15. Simulation 8. (a) Volumetric gas fraction and flow pattern of liquid water at shallow depths and at different times. Contour lines every 0.005, from 0.02 to 0.065. Maximum flow rate for liquid water is 1.02×10^{-4} kg/m^2 s. Different patterns indicate different lithologies, as shown in Fig. 3, and highlight the gap through the Clay layer at depth. (b) Temperature (°C) distribution at steady state . Contour lines every 10°C, from 30 to 140°C. (c) Gas flow rate through the surface at different times. The thick, black line indicates the extent of the two-phase zone

Fig. 16. Simulations 7 & 8. Distribution of (a) CO_2 partial pressure (MPa), (b) temperature (°C), and (c) volumetric gas fraction with depth, along the symmetry axis, for the cases of structural high and low. Dashed lines indicate the vertical profiles at the beginning of the simulations (shown in Fig. 7), while solid lines indicate steady state values.

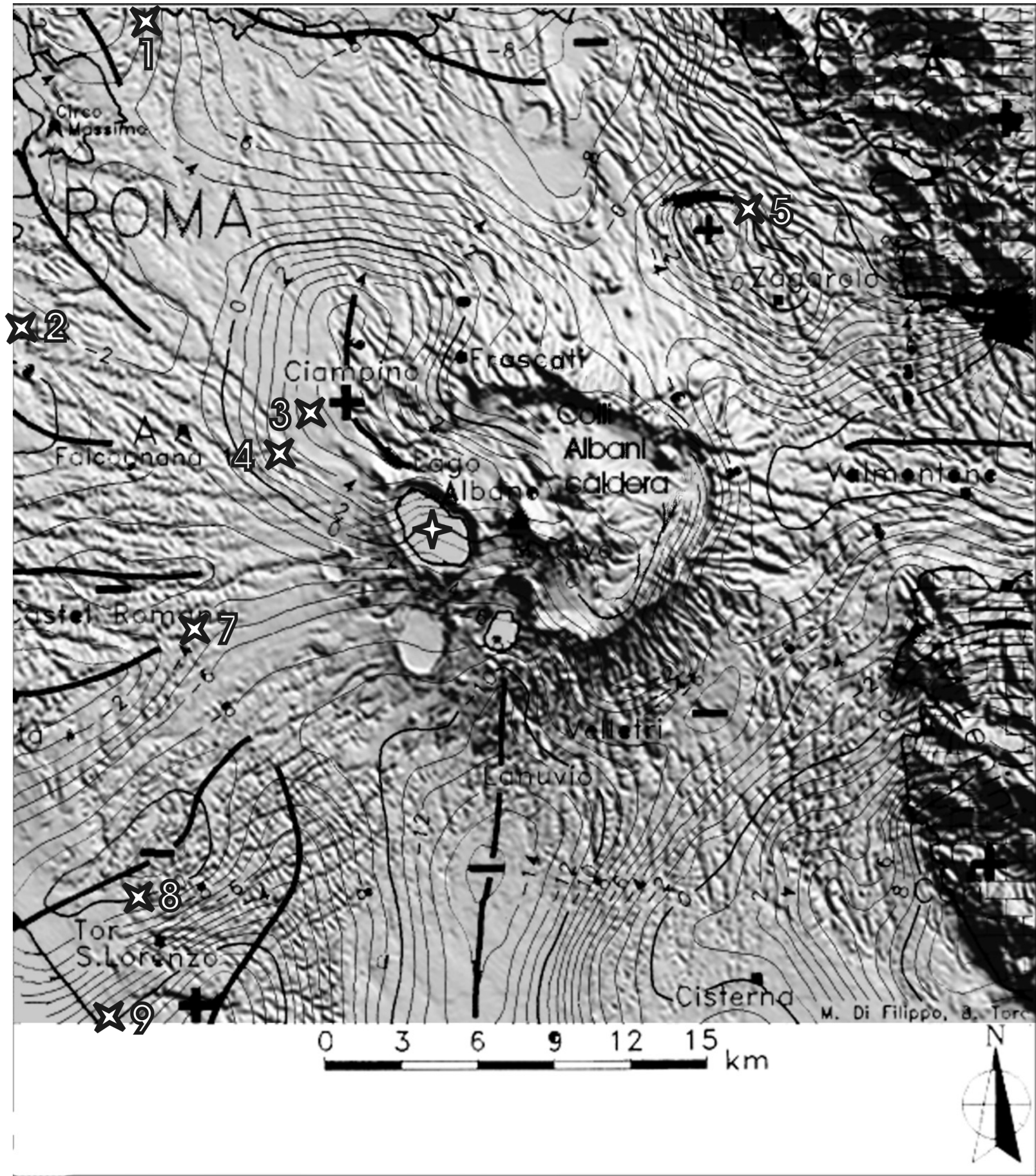
1
Circo Massimo
ROMA
2
Ciampino
Frascati
Zagarolo
3
Colli Albani caldera
4
Falcognana
Lago Albano
Velletri
5
Valmontone
7
Castel Romano
Lanuvio
8
Tor S.Lorenzo
9
Cisterna
M. Di Filippo, A. Torc
0 3 6 9 12 15 km
N

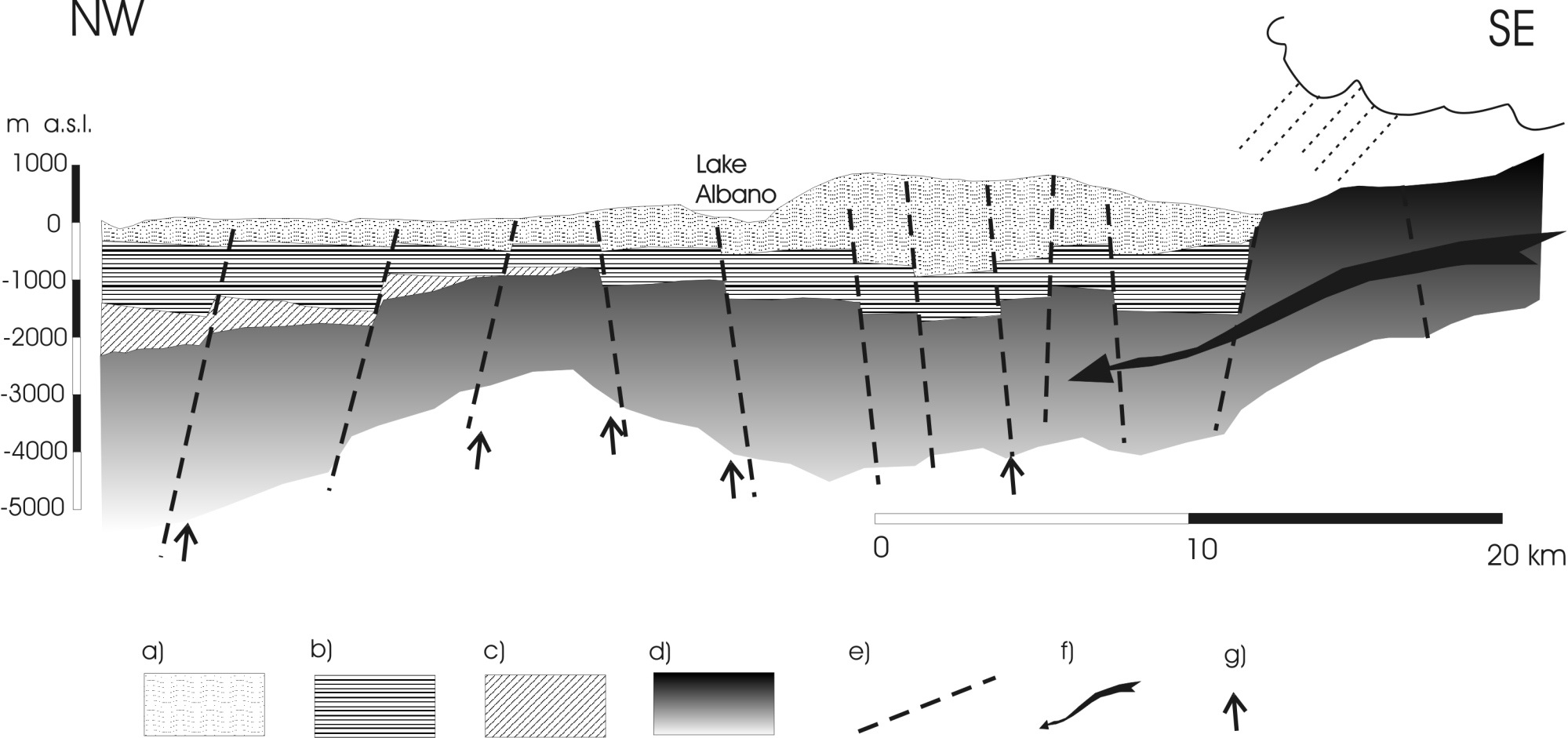
NW
SE
m a.s.l.
1000
0
-1000
-2000
-3000
-4000
-5000
Lake
Albano
0
10
20 km
a)
b)
c)
d)
e)
f)
g)

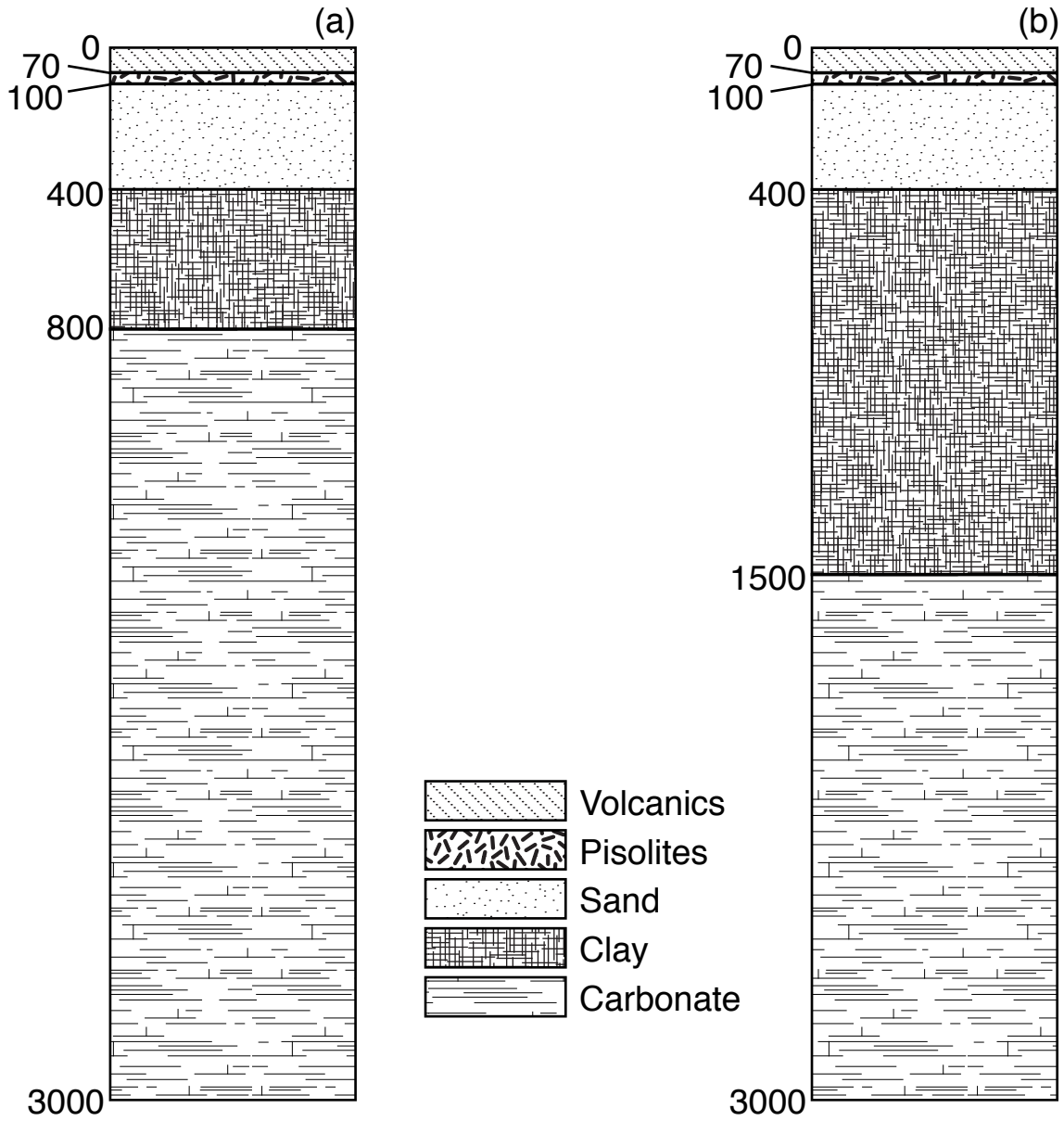
(a)
0
70
100
400
800
3000
(b)
0
70
100
400
1500
3000
Volcanics
Pisolites
Sand
Clay
Carbonate

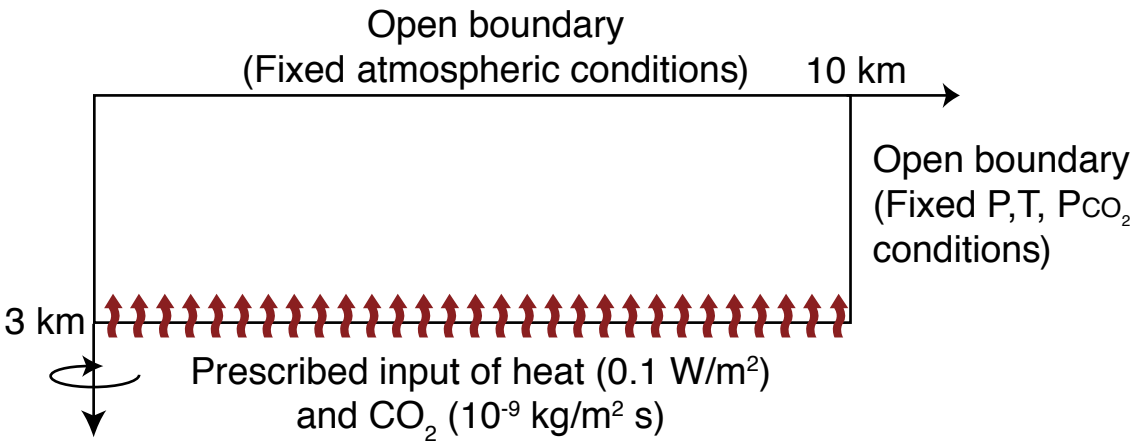
Open boundary
(Fixed atmospheric conditions)
10 km
Open boundary
(Fixed P,T, P_{CO_2}
conditions)
3 km
Prescribed input of heat (0.1 W/m^2)
and CO_2 (10^{-9} kg/m^2 s)

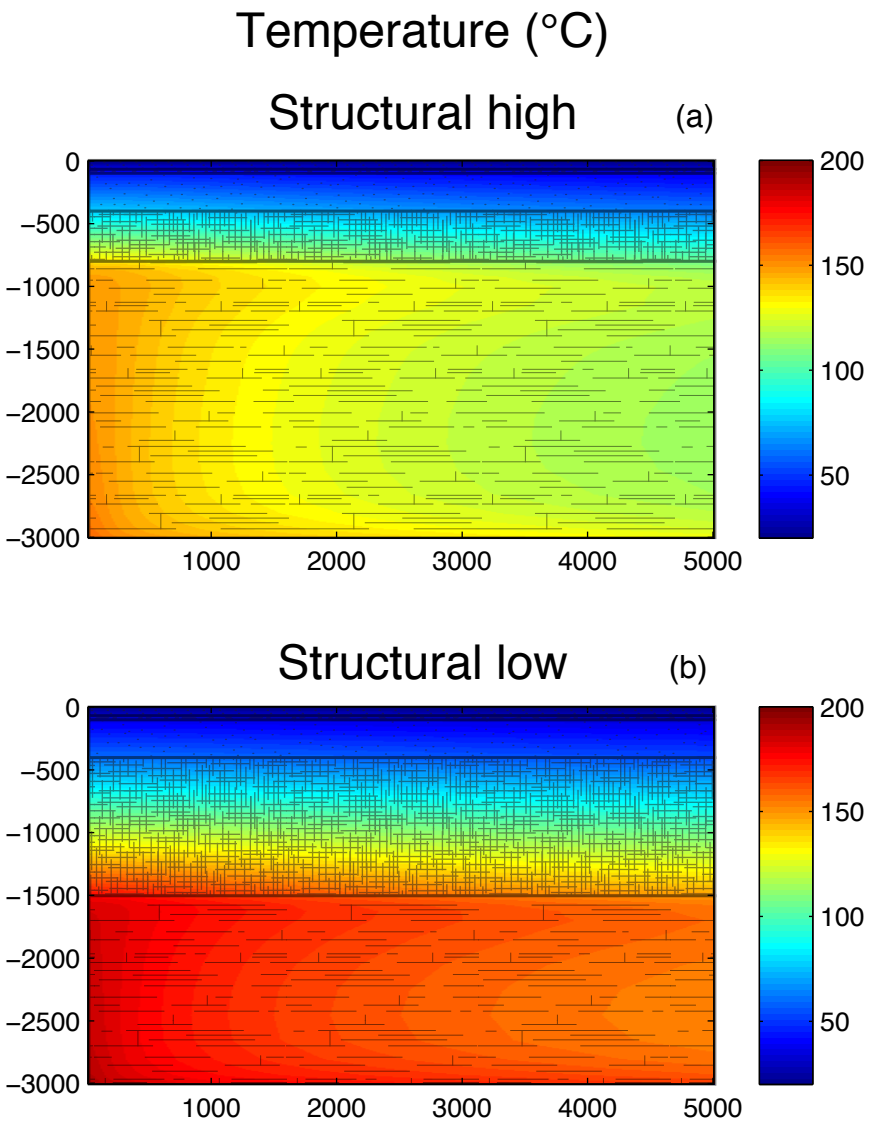
Temperature (°C)
Structural high
(a)
0
−500
−1000
−1500
−2000
−2500
−3000
1000
2000
3000
4000
5000
200
150
100
50
Structural low
(b)
0
−500
−1000
−1500
−2000
−2500
−3000
1000
2000
3000
4000
5000
200
150
100
50

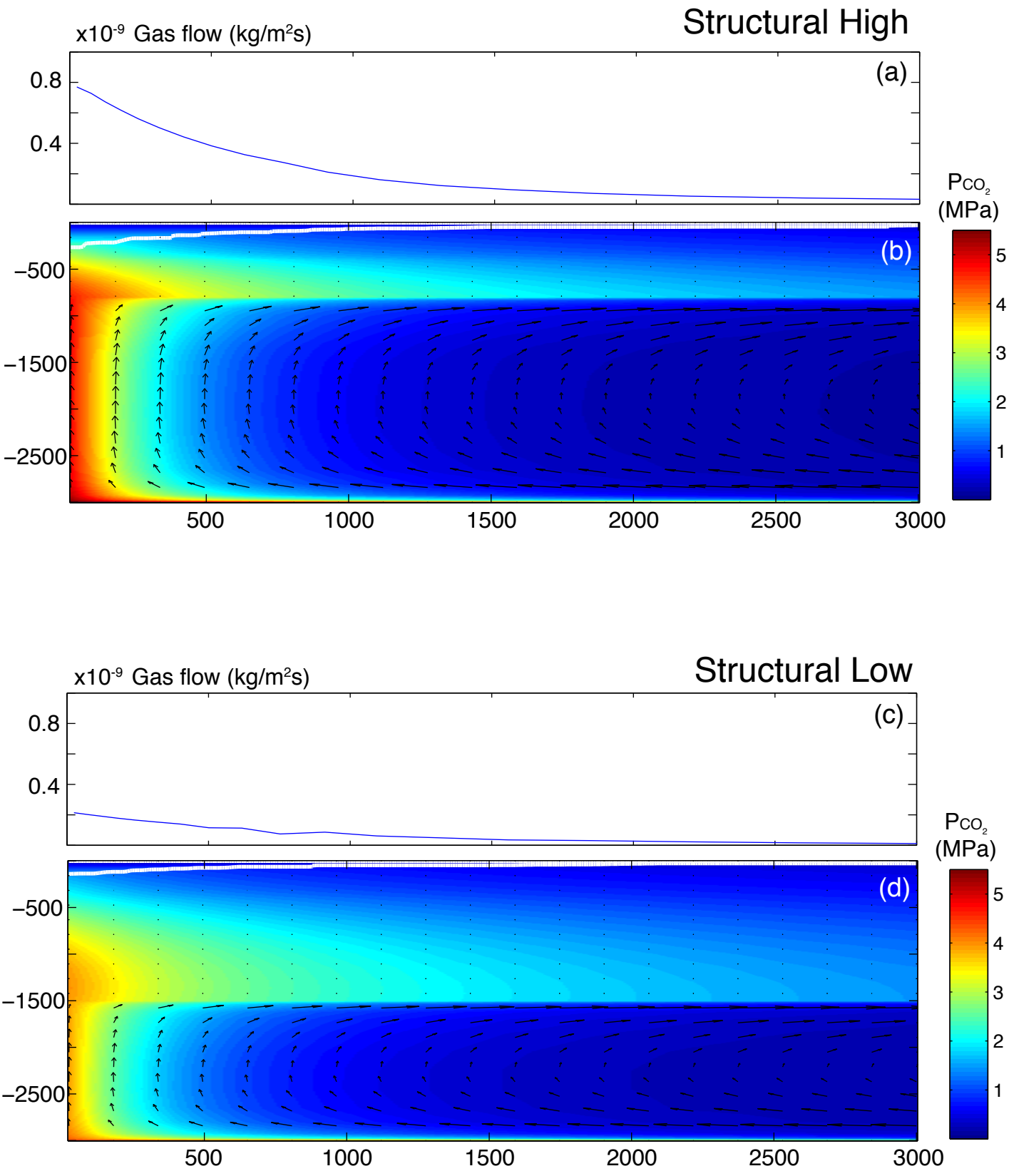
Structural High
x10-9 Gas flow (kg/m2s)
0.8
0.4
(a)
(b)
−500
−1500
−2500
500
1000
1500
2000
2500
3000
PCO2 (MPa)
5
4
3
2
1
Structural Low
x10-9 Gas flow (kg/m2s)
0.8
0.4
(c)
(d)
−500
−1500
−2500
500
1000
1500
2000
2500
3000
PCO2 (MPa)
5
4
3
2
1

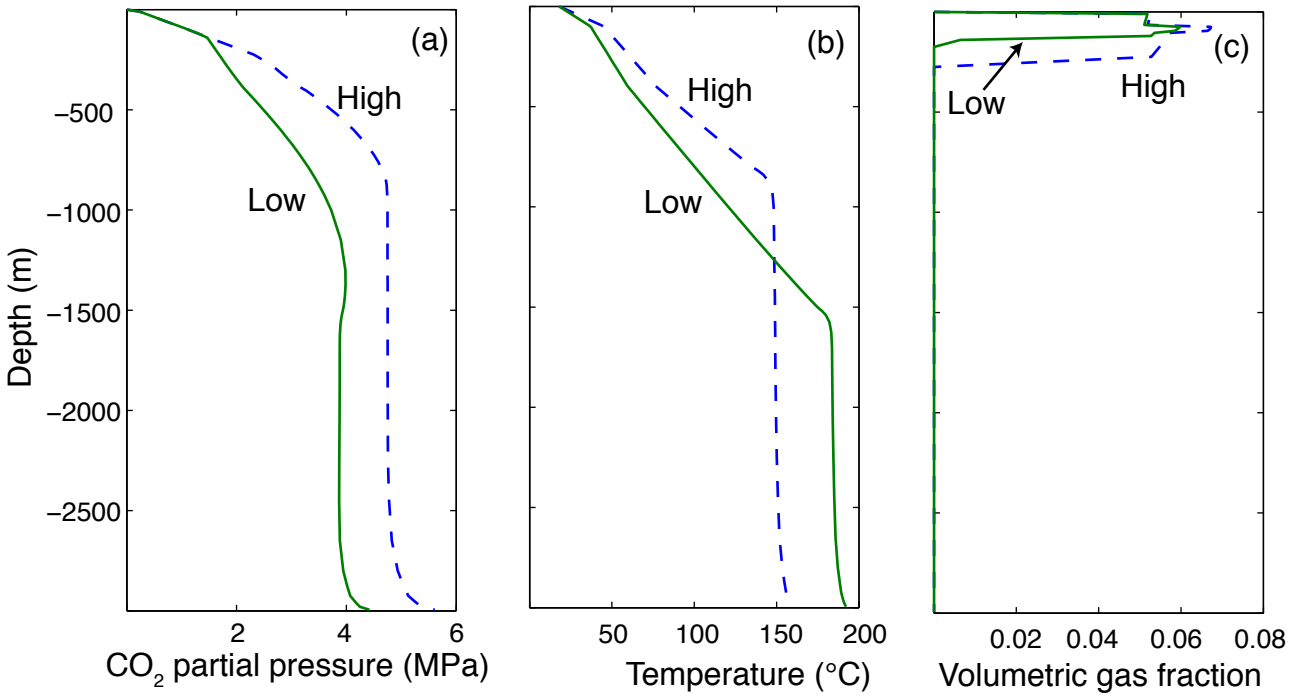
(a)
High
Low
−500
−1000
−1500
−2000
−2500
Depth (m)
2
4
6
CO2 partial pressure (MPa)
(b)
High
Low
50
100
150
200
Temperature (°C)
(c)
Low
High
0.02
0.04
0.06
0.08
Volumetric gas fraction

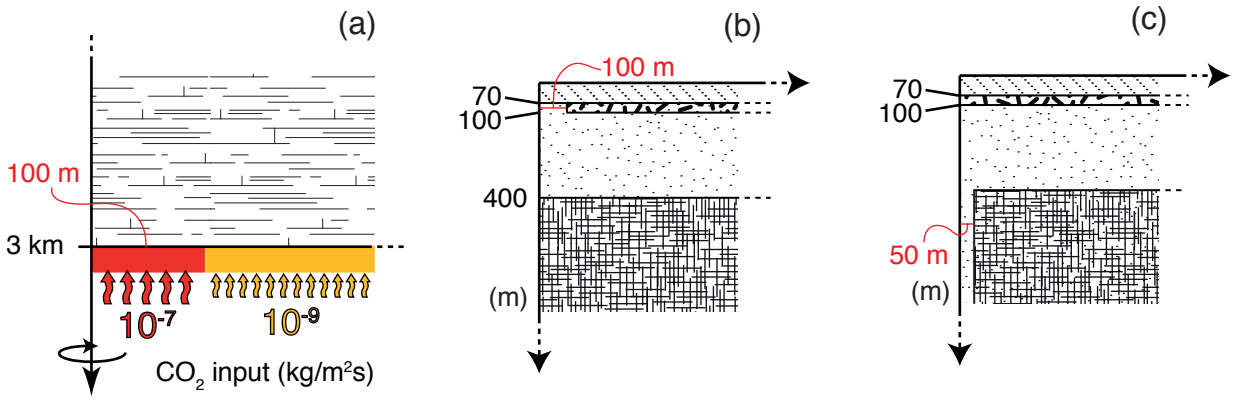
(a)
100 m
3 km
10^{-7}
10^{-9}
CO_2 input (kg/m^{2}s)
(b)
100 m
70
100
400
(m)
(c)
70
100
50 m
(m)

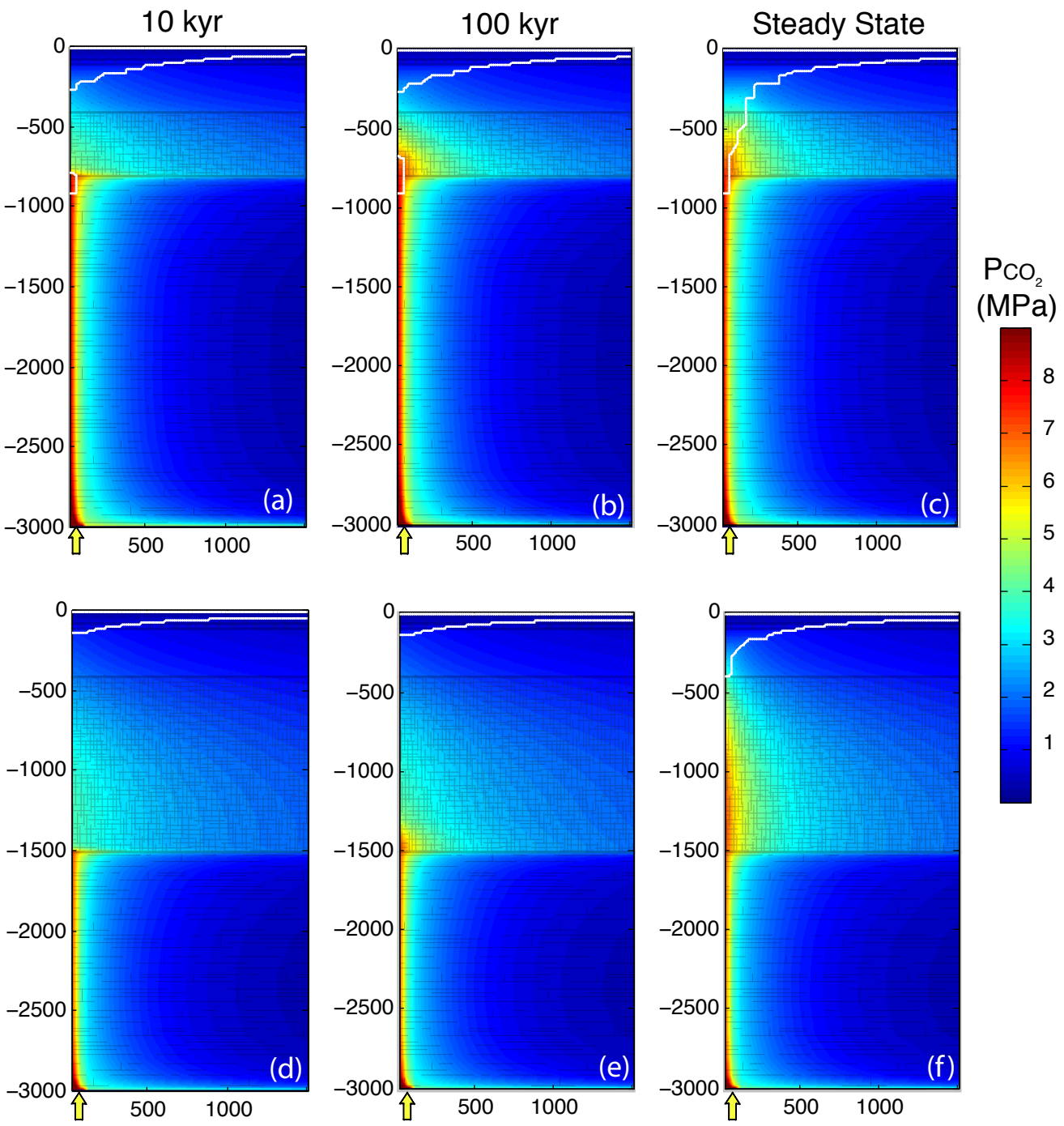
10 kyr
100 kyr
Steady State
0
−500
−1000
−1500
−2000
−2500
−3000
500
1000
(a)
(b)
(c)
(d)
(e)
(f)
PCO2 (MPa)
8
7
6
5
4
3
2
1

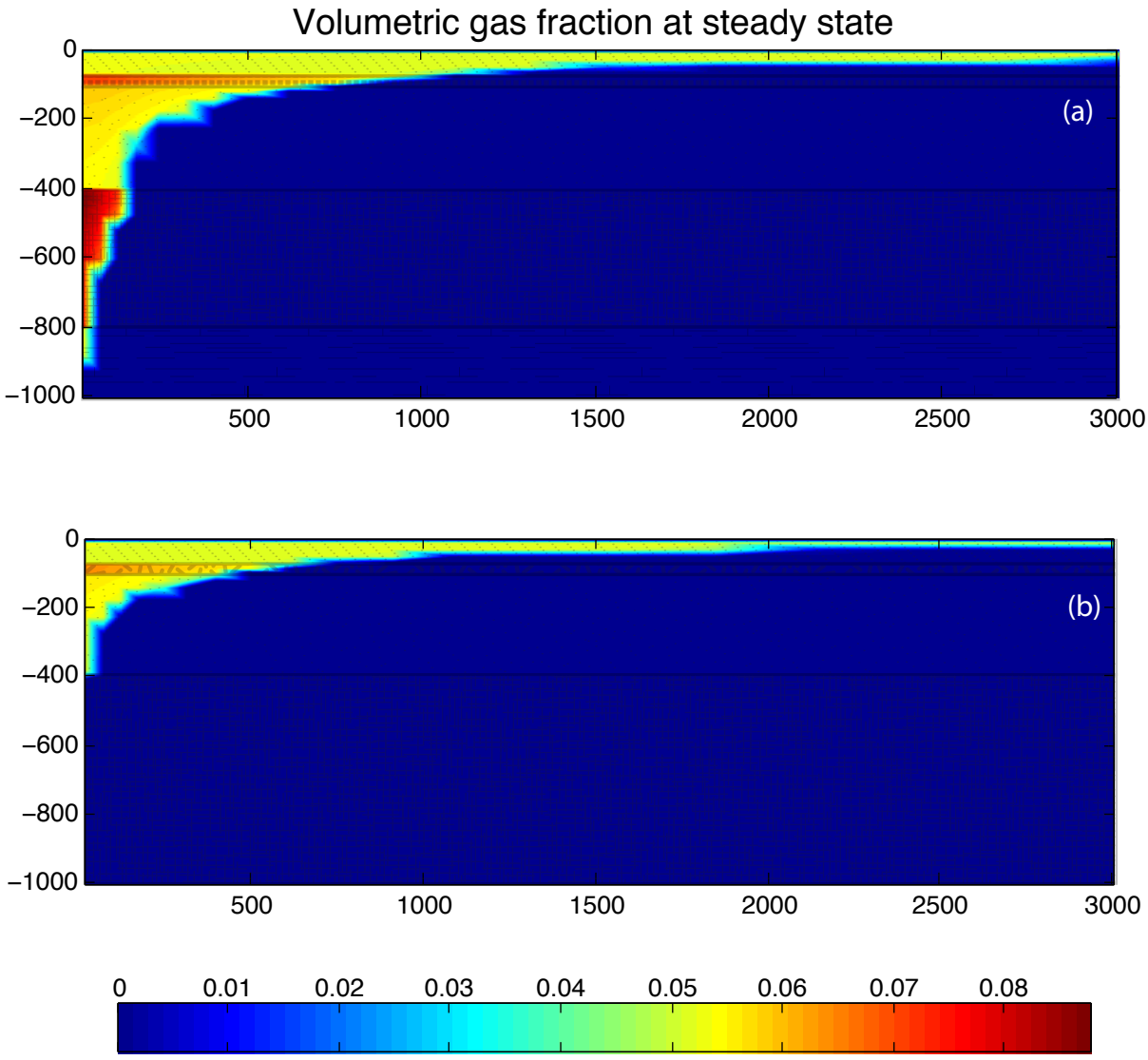
Volumetric gas fraction at steady state
0
−200
−400
−600
−800
−1000
500
1000
1500
2000
2500
3000
(a)
(b)
0
0.01
0.02
0.03
0.04
0.05
0.06
0.07
0.08

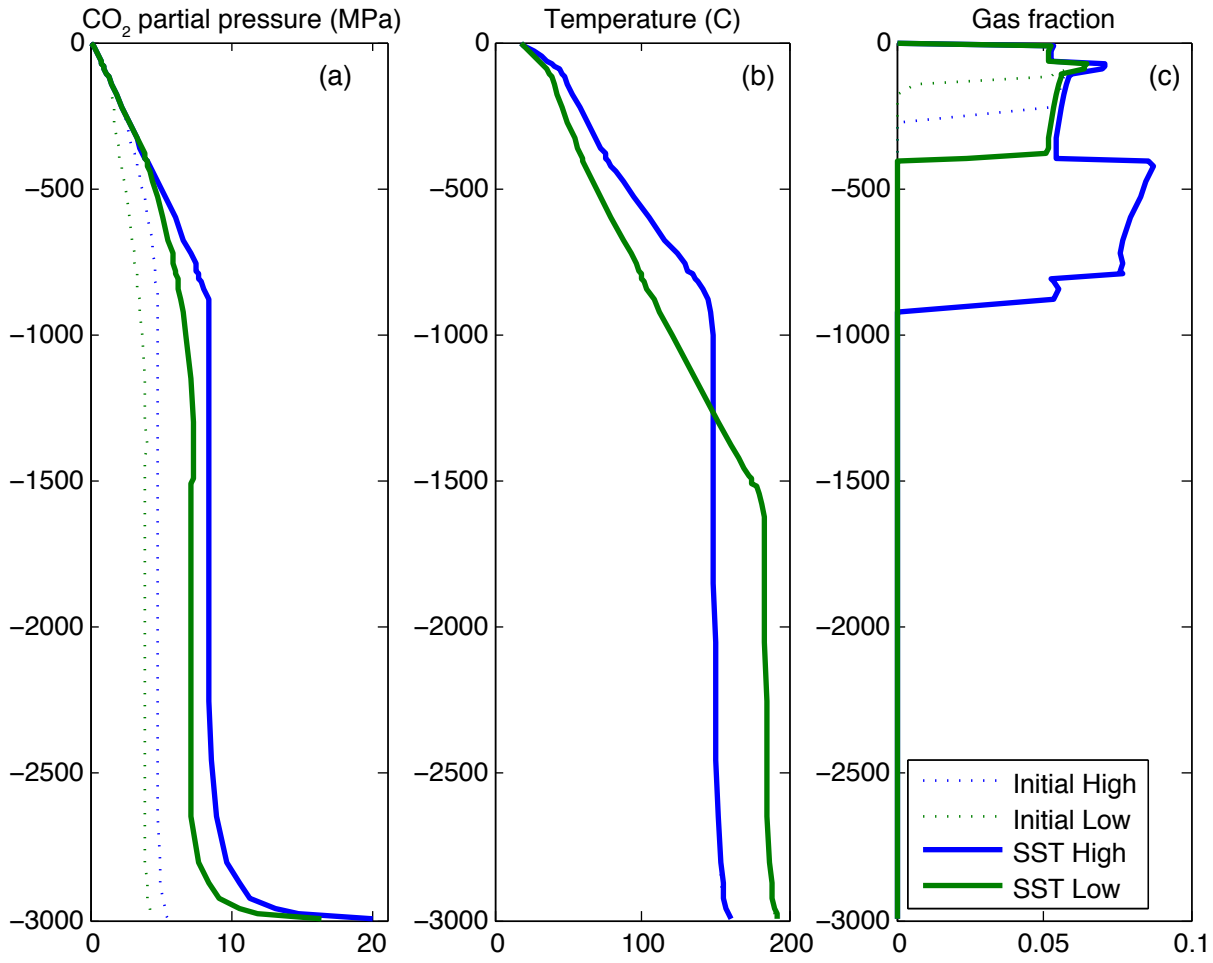
CO_2 partial pressure (MPa)
Temperature (C)
Gas fraction
(a)
(b)
(c)
0
−500
−1000
−1500
−2000
−2500
−3000
0
10
20
100
200
0.05
0.1
Initial High
Initial Low
SST High
SST Low

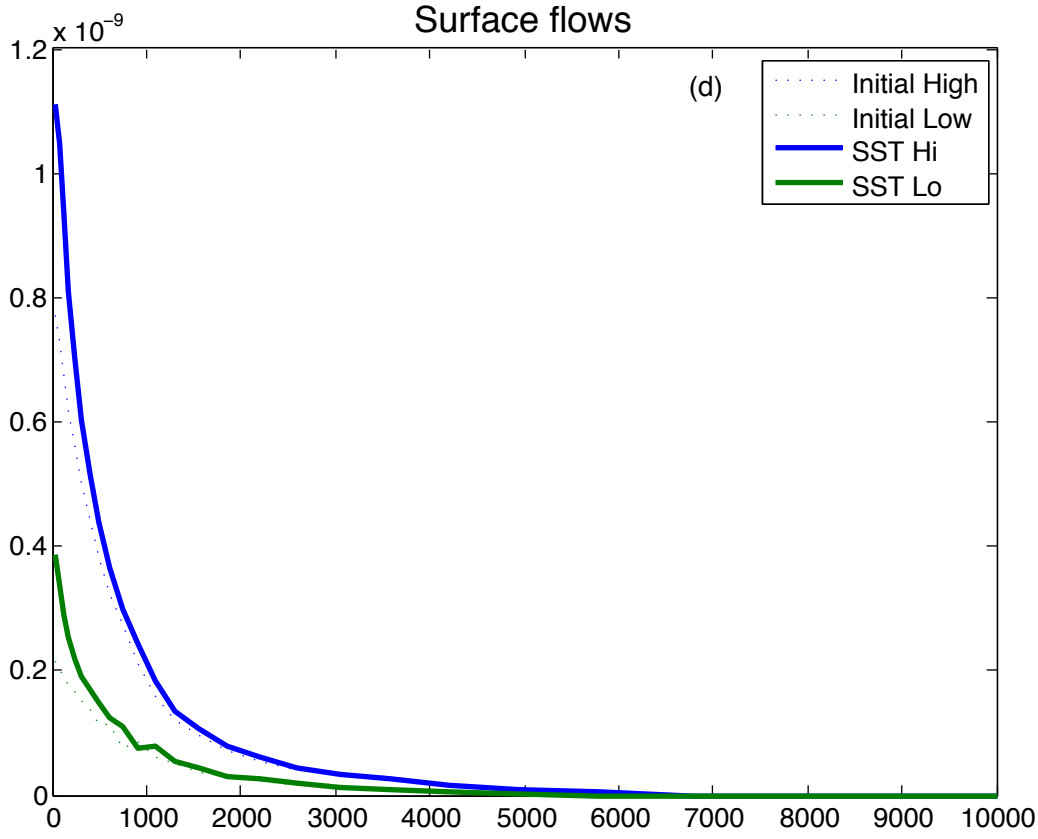
Surface flows
x 10^{-9}
(d)
1.2
1
0.8
0.6
0.4
0.2
0
0
1000
2000
3000
4000
5000
6000
7000
8000
9000
10000
Initial High
Initial Low
SST Hi
SST Lo

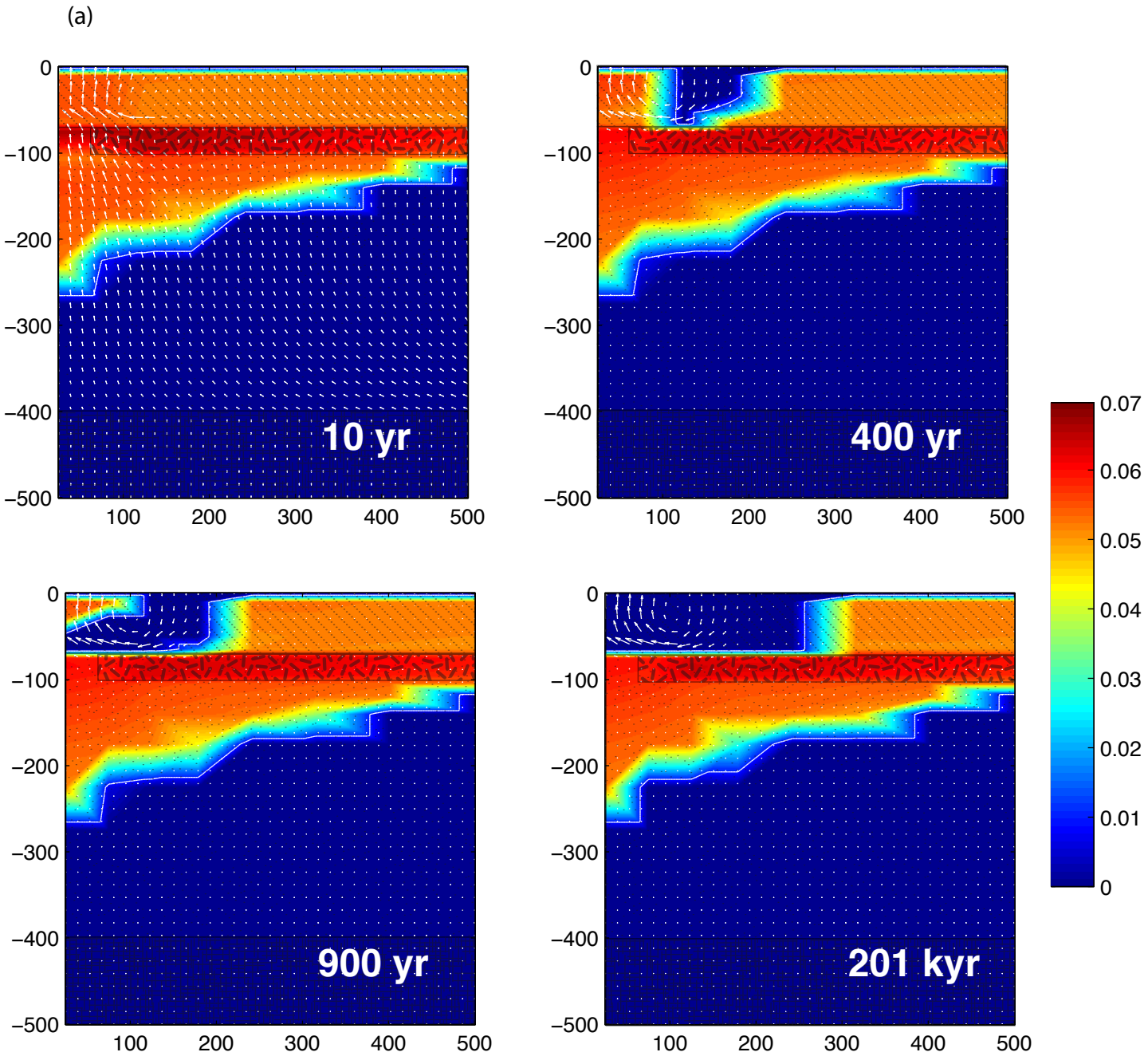
(a)
10 yr
400 yr
900 yr
201 kyr
0
−100
−200
−300
−400
−500
100
200
300
400
500
0.07
0.06
0.05
0.04
0.03
0.02
0.01
0

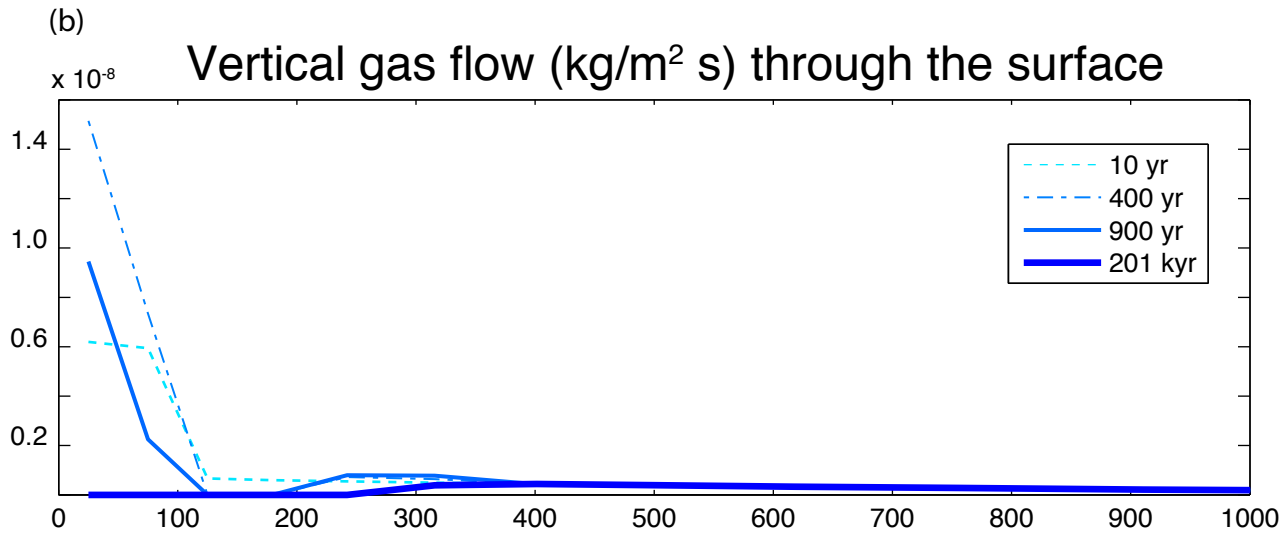
(b)
Vertical gas flow (kg/m² s) through the surface
x 10⁻⁸
1.4
1.0
0.6
0.2
0
100
200
300
400
500
600
700
800
900
1000
10 yr
400 yr
900 yr
201 kyr

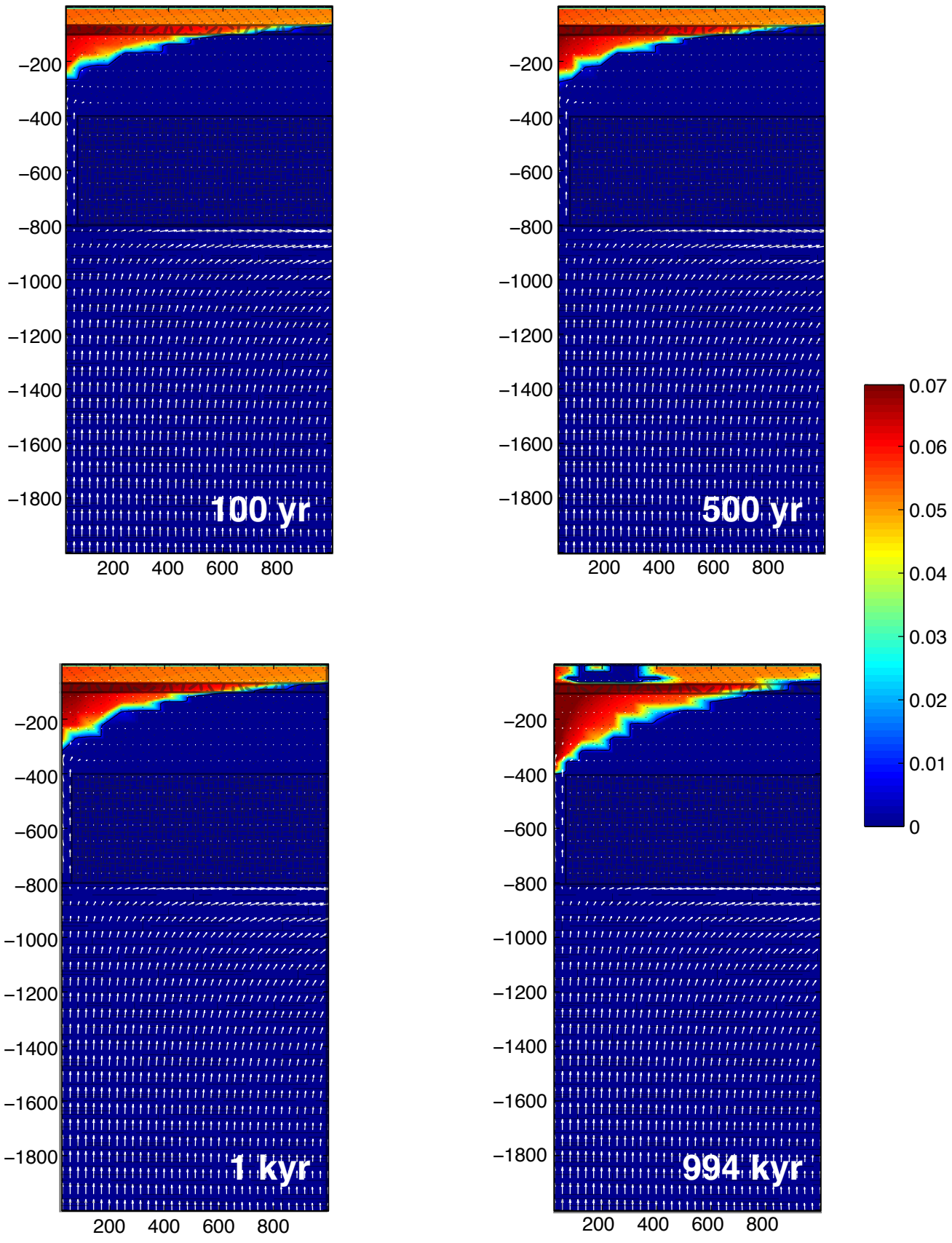
−200
−400
−600
−800
−1000
−1200
−1400
−1600
−1800
200
400
600
800
100 yr
500 yr
1 kyr
994 kyr
0.07
0.06
0.05
0.04
0.03
0.02
0.01
0

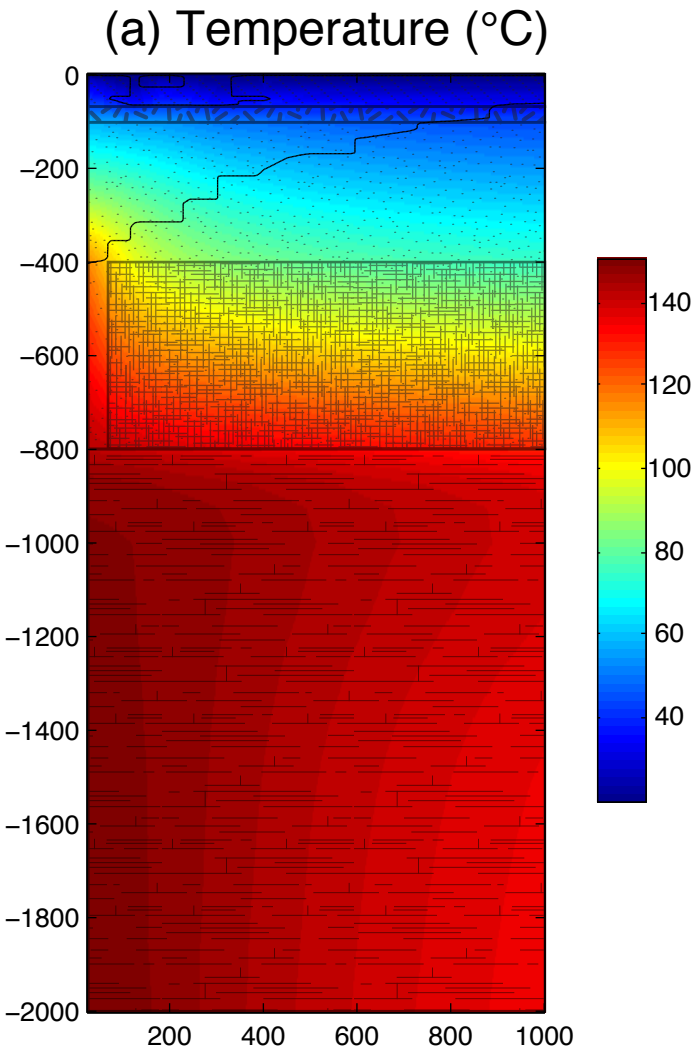
(a) Temperature (°C)
0
−200
−400
−600
−800
−1000
−1200
−1400
−1600
−1800
−2000
200
400
600
800
1000
140
120
100
80
60
40

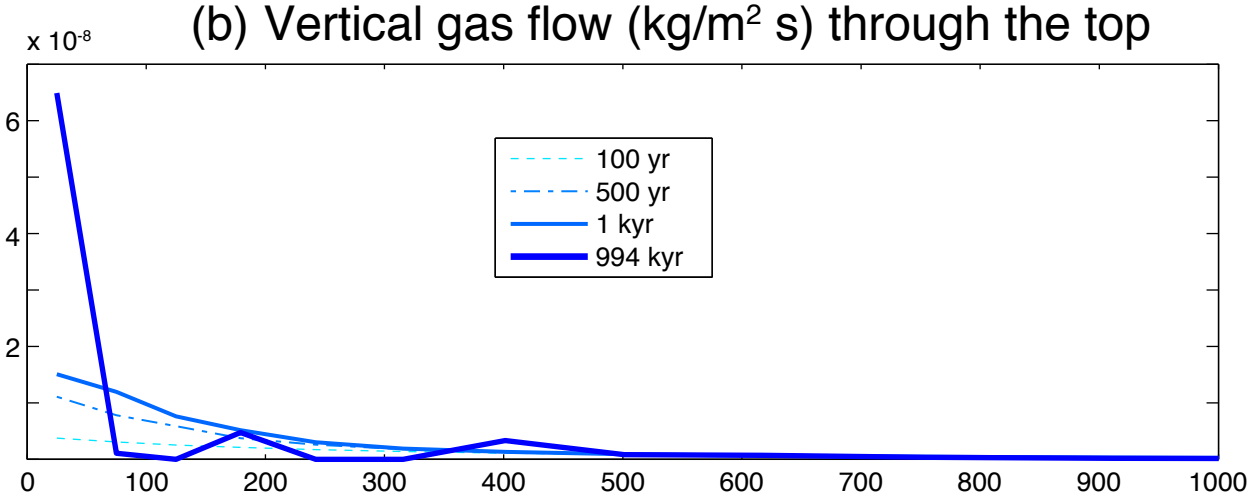
(b) Vertical gas flow (kg/m² s) through the top
x 10⁻⁸
6
4
2
0
100
200
300
400
500
600
700
800
900
1000
100 yr
500 yr
1 kyr
994 kyr

(a) Volumetric gas fraction

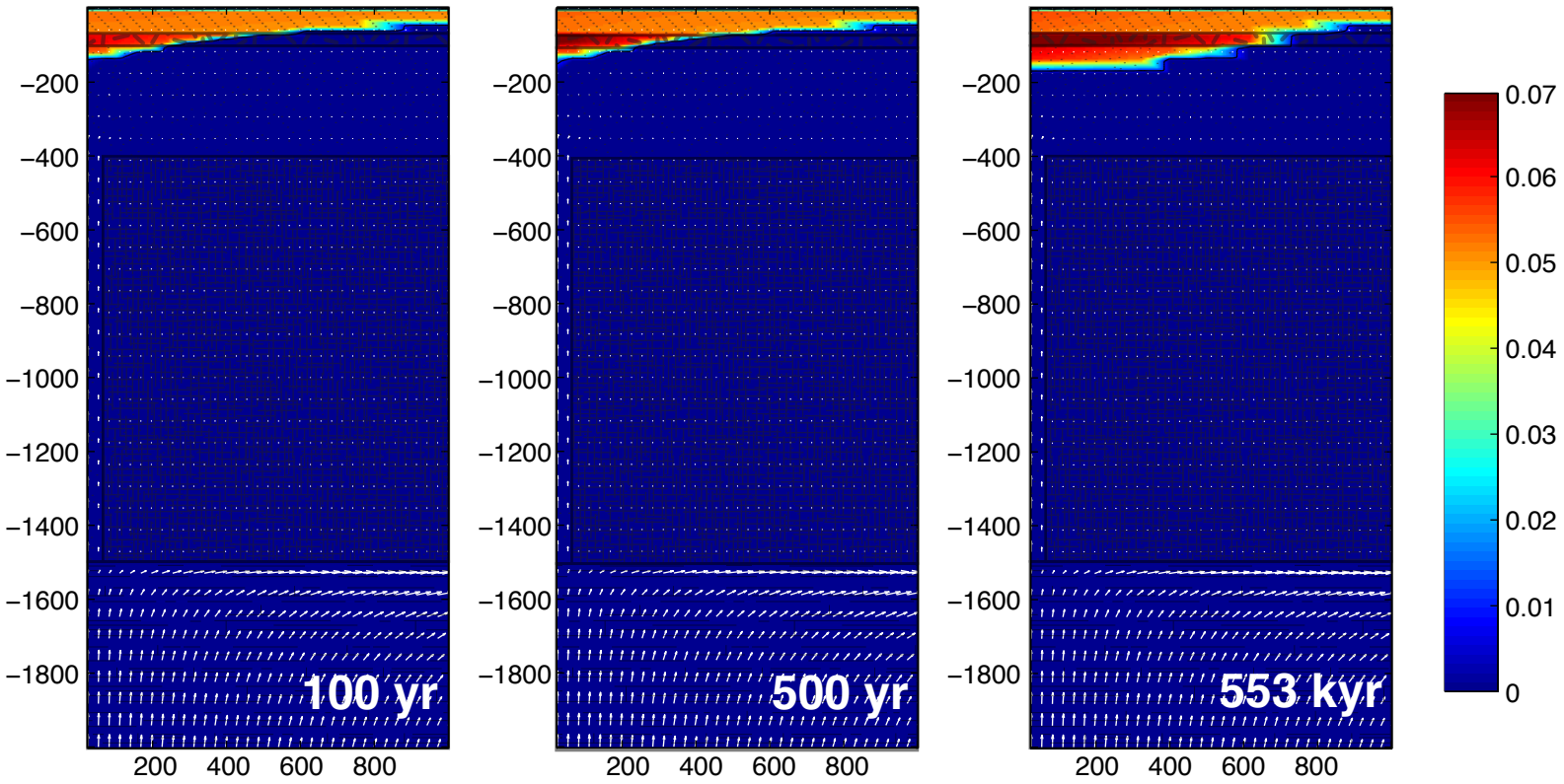

(b) Temperature (°C)

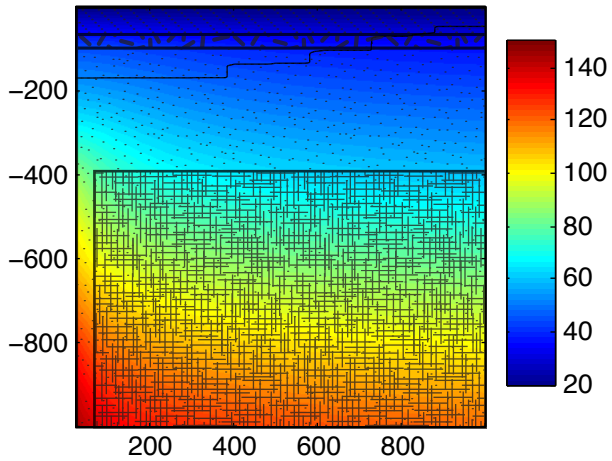

(c) Vertical gas flow (kg/m^2 s) through the top

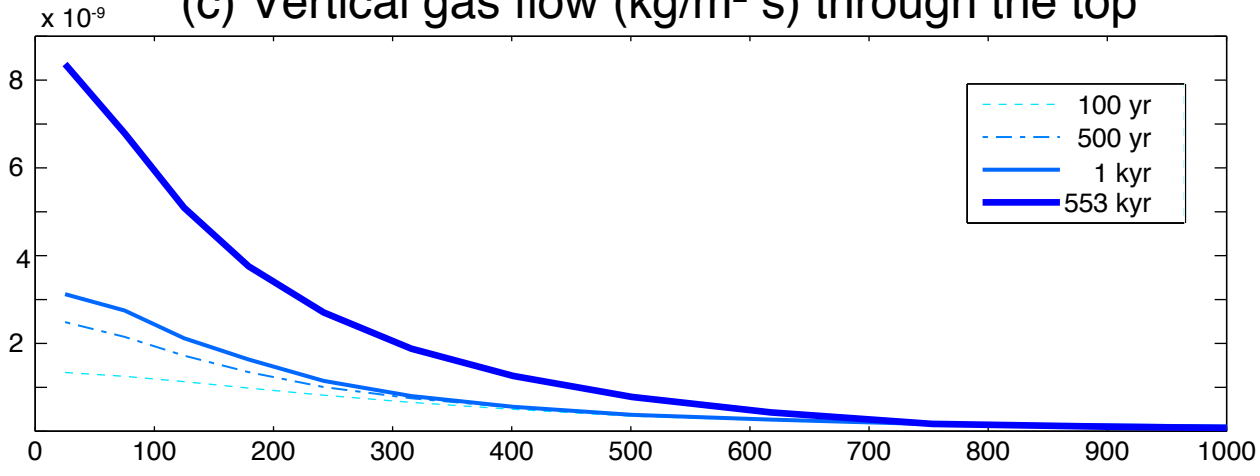

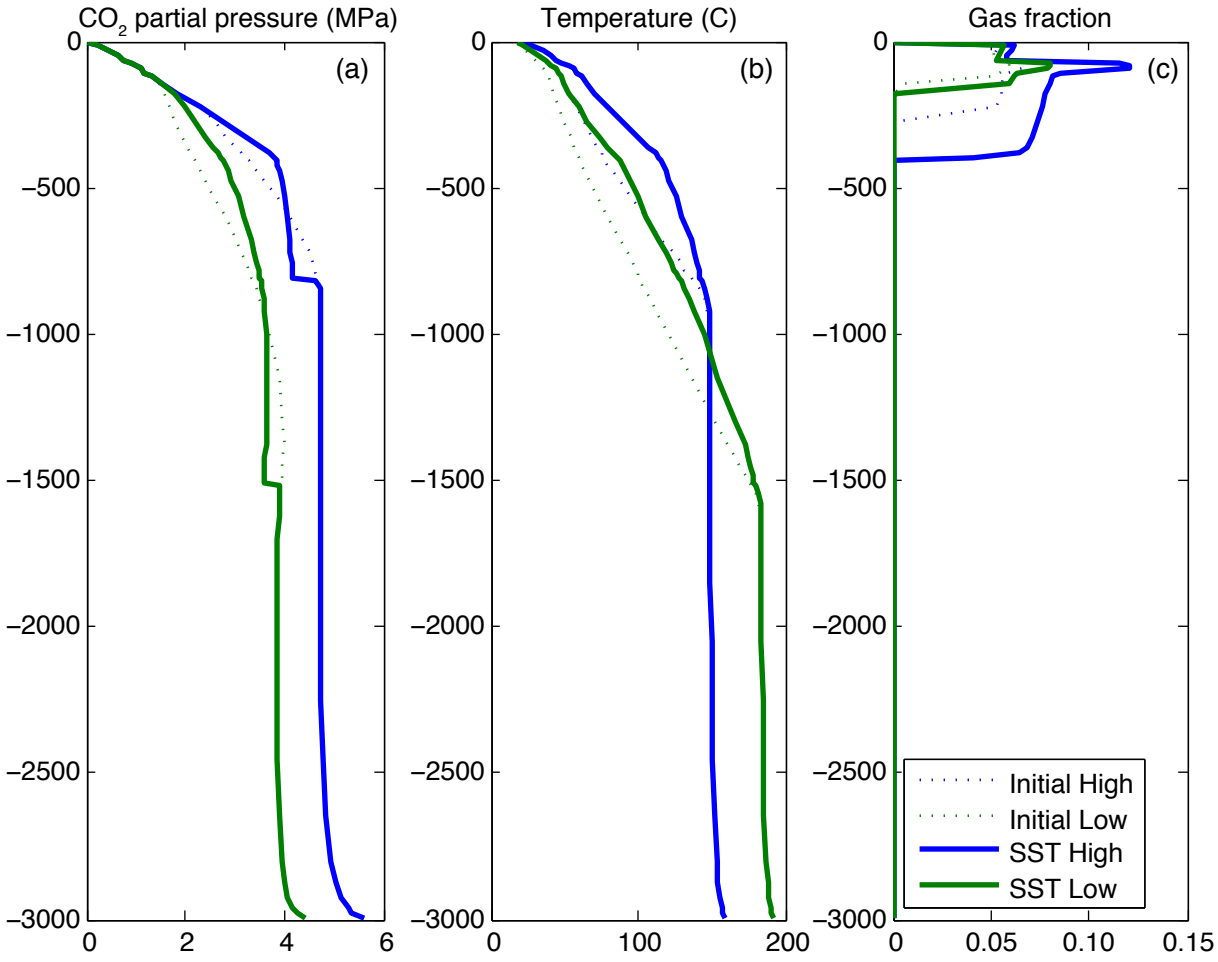
CO_2 partial pressure (MPa)
Temperature (C)
Gas fraction
(a)
(b)
(c)
0
−500
−1000
−1500
−2000
−2500
−3000
0
2
4
6
100
200
0.05
0.10
0.15
Initial High
Initial Low
SST High
SST Low